International Journal of Lightweight Materials and Manufacture 2 (2019) 146–155

Contents lists available at ScienceDirect

International Journal of Lightweight Materials and Manufacture

journal homepage: https://www.sciencedirect.com/journal/international-journal-of-lightweight-materials-and-manufacture

Original Article

Cohesive surface model for delamination and dynamic behavior of hybrid composite with SMA-GFRP interface

Aaqib Ali [a, *, 1], Antonietta Lo Conte [a], Carlo Alberto Biffi [b], Ausonio Tuissi [b]

[a] Politecnico di Milano, Department of Mechanical Engineering, via La Masa 1, 20156, Milan, Italy
[b] CNR-ICMATE, Corso Promessi Sposi 29, 23900, Lecco, Italy

ARTICLE INFO

Article history:
Received 4 December 2018
Received in revised form
25 January 2019
Accepted 26 January 2019
Available online 8 February 2019

Keywords:
Hybrid composite
Delamination
FE analysis
Cohesive interface
Damage initiation
Modal dynamics

ABSTRACT

The interface model between *CuZnAl* SMA and GFRP, used in a hybrid composite, is proposed using cohesive surfaces. Using this model and derived parameters, mode-II delamination is studied between *CuZnAl* SMA insert and GFRP and also between laser patterned *CuZnAl* SMA insert and GFRP. Natural frequency and damping ratio of the hybrid composite specimen, in the shape of slender beam in a cantilever configuration, are evaluated in impulse tests. A numerical model is also presented, to calculate the aforementioned dynamic properties numerically, using Modal Strain Energy (MSE) and Modal Dynamics procedures by considering the derived interfacial parameters.

1. Introduction

By using Shape Memory Alloy (SMA) material in hybrid composite, different properties of interest like large recoverable strain, fatigue, creep, stress recovery, damping, etc. can be improved [1]. A number of hybrid composites have been presented in literature having SMA as the reinforcement or the matrix [2]. Out of these, hybrid composite of Glass Fiber Reinforced Polymer (GFRP) with SMA sheet inserts, is specially significant owing to its broad usage in engineering applications by utilizing its low weight, rigidness and high energy dissipation characteristics [3].

Shape memory alloys have unique damping property, owing to the internal damping of the martensitic phase. High inherent damping of such martensitic phase has been linked to the motions of atoms and defects and the under stress re-orientation of martensite twin variants [4]. From a practical view point, this intrinsic mechanism of energy dissipation, over wide temperature range, provides an attractive outlook for the utilization of shape memory alloys as passive dampers for low amplitude mechanical vibrations in automobile, aerospace, railway and other dynamic applications. The most widely studied SMA materials for increasing the structural damping are Nitinol (*NiTi*), *NiTiCu*, *CuAlNi* and *CuZnAl* alloys.

The *CuZnAl*-GFRP hybrid composite turns out to be more attractive due to the following reasons. *CuZnAl* alloy exhibits the highest structural damping among these high damping alloys [5,6] and also a comparatively high and appropriate elastic modulus. For the lateral horns of a railway pantograph's collectors, a new hybrid composite having shape memory allow insert was proposed in Ref. [7]. The basic purpose of this proposal was to increase the structural damping of the widely used GFRP structures without significantly modifying its compliance and weight, also considering manufacturability and economics for engineering applications. *CuAlZn* SMA sheets with low thickness were proposed as inserts in a GFRP host composite. These low thickness inserts were laser patterned to enhance the load transfer between the host composite and the inserts, and to prevent delamination at the SMA-GFRP interface. The area ratio of the micro-cuts and the remaining sheet area, and the effect of the laser cutting, were previously investigated in Ref. [8]. The hole pattern geometry, the ratio between the total holes surface area and the total SMA sheet surface area, and the sheet's thickness, were optimized to ensure that the overall weight and natural frequency of the structure were

* Corresponding author.
E-mail address: aaqib_124@hotmail.com (A. Ali).
Peer review under responsibility of Editorial Board of International Journal of Lightweight Materials and Manufacture.
[1] Present address: GIK Institute of Engineering Sciences & Technology, 23640, Topi, Pakistan.

https://doi.org/10.1016/j.ijlmm.2019.01.006

preserved. The effects of laser patterning on transformation temperatures and internal friction properties of the SMA were also analyzed. The selection of SMA *CuZnAl*, as insert material, and the chosen architecture provided the most cost effective option without special purpose-built devices, but the problem of the interface strength and the effectiveness of the proposed solution to avoid delamination, was still open.

The intended function of SMA based hybrid composites can not be ensured without the full knowledge of their stress transfer properties and interfacial adhesive behavior, between the constituents. The strength of the insert exceeds considerably the strength of the host composite and, thus, the interface is responsible for the load transfer between the two constituents of the hybrid composite. As soon as the shear stress between the constituents rises to the level of shear strength of the interface, interfacial delamination/debond will start right away. The greater is the interfacial shear strength, the stronger the hybrid composite material will be. Different parameters are used to characterize the interface between the reinforcement and the matrix in a composite material, like normal and shear interfacial strength, critical energy release rate, frictional shear stress and the coefficient of friction between the contacting surfaces. Various kinds of micro-mechanical tests have been developed to obtain experimental data related to these parameters.

In Ref. [9], the interfacial strength between GFRP and *CuZnAl* sheet was investigated through pull-out tests. The effect of the micro-cuts in the SMA sheet on the interfacial load transferability was studied. The results proved that the improvement in the gross load transfer capacity and interfacial strength, due to the existence of micro-cuts, is quite significant than the reduction due to the decreased contact area between the insert and the matrix.

This paper presents a cohesive surface based model which can be used to study in detail the effects of different micro-cut patterns on the load transfer mechanism at the interface of SMA/GFRP. The proposed cohesive model is applied successfully to simulate, by finite element numerical analysis, the experimental dynamic behavior of a composite beam in which the investigated patterned interface has been used. It must be noted that the post crack initiation regime and crack propagation behavior is not studied and discussed here.

The methodology for the present study is briefly explained which will help to understand this article better. First of all, pull-out test was performed on the hybrid composite specimen with plain SMA insert. The results of this experiment were used to calculate and, after comparison of experimental and numerical results, calibrate the interfacial parameters for numerical model. These parameters were used to model the hybrid composite specimen with SMA insert with micro-cuts and the results were compared to another set of pull-out experiments for validation of the numerical model.

Experiments were performed to find out the damping and natural frequency of a bean specimen made of hybrid composite. A numerical model was set up with the derived interfacial parameters and then a modal dynamics study was performed to numerically calculate the damping and natural frequency. On comparing the experimental and numerical results, the interfacial parameters calculated were further verified. All the simulations were carried out with *Abaqus* code.

2. SMA-GFRP hybrid composite architecture and materials

In Fig. 1a, the basic architecture of the proposed SMA-GFRP hybrid composite is presented. A thick core of GFRP $[+45/-45]_n$ is sandwiched between two thin layers of patterned *CuZnAl* SMA with thin layers of GFRP $[+45/-45]_2$ on top and the bottom. The thin SMA inserts are patterned by laser with elliptical micro-cuts according to the schematic of Fig. 1b and further details are mentioned in Ref. [7].

The GFRP is uni-directional S2 Glass/125 °C curing epoxy resin, manufactured by 3 M (SP250 S29A). The SMA alloy is $Cu_{66}Al_{24}Zn_{10}$, with characteristic transformation temperatures: $M_f = 50°C$, $M_s = 63°C$; $A_s = 60°C$, $A_f = 68°C$. Young's modulus and Poisson's ratio, for GFRP plied $[+45/-45]_n$ and for $Cu_{66}Al_{24}Zn_{10}$ SMA alloy, are given in Table 1, together with the density values.

3. Experiments

3.1. Pull-out tests

The pull-out tests were performed at room temperature by means of an Instron electro-mechanical testing machine with 10 kN load cell. The specimen used for the pull-out tests is shown in Fig. 2a, along with shape and dimensions. The schematic illustration of the test is shown in Fig. 2b, details are reported in Ref. [9]. The specimen was put in a metallic holder with a thin slit in the center to align the sheet with the axis of the holder. The open end of the SMA was fixed at the lower grips of the machine and the tensile load at the rate of 1 mm/min was applied with the help of upper

Table 1
Material properties.

Material	Young's modulus [GPa]	Poisson's ratio	Density [kg/m]^3
GFRP $[+45/-45]_n$	16.5	0.35	1880
$Cu_{66}Al_{24}Zn_{10}$	78.0	0.20	7400

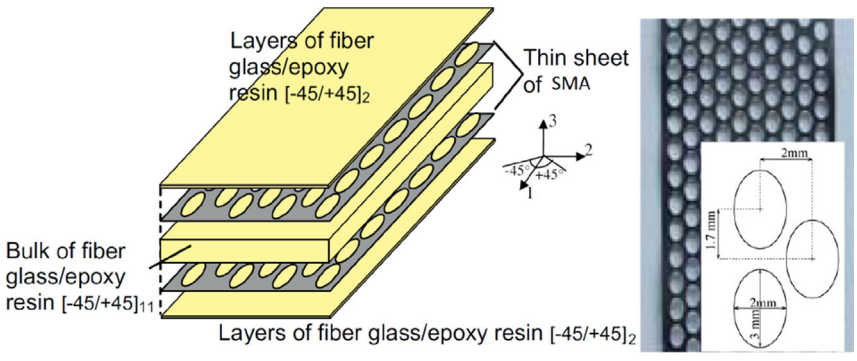

Fig. 1. (a) Architecture of the SMA-GFRP hybrid composite. (b) Geometry of the elliptical micro-cuts for the laser pattern of the SMA inserts.

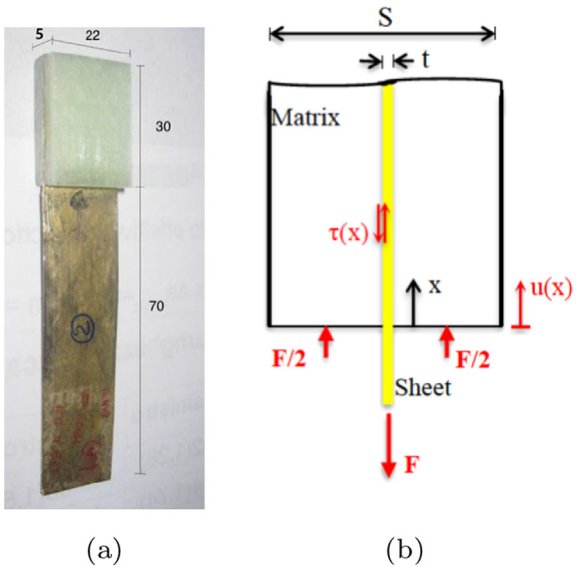

Fig. 2. (a) Hybrid composite specimen for pull-out test (dimensions in mm). (b) Schematic illustration of the pull-out test.

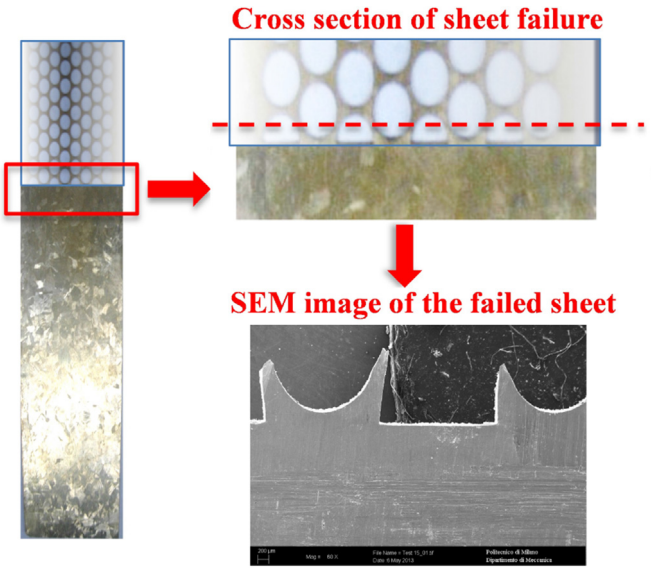

Fig. 4. Detail of the failure of SMA in the hybrid composite during the pull-out test with elliptical holes patterned sheet insert.

grips. The data of load (F) as a function of displacement ($u(x)$) of the lower end of the GFRP was recorded. The GFRP bulk was $[+45/-45]_{16}$ plied. Plain SMA sheet and sheet with micro-cuts were used in the tests, all with the thickness of 0.3 mm, and three specimens were tested for each configuration.

The force-displacement curves obtained as a result of pull-out tests for both kinds of specimens, are shown in Fig. 3. It can be observed that, despite of the reduction in the interface/contact area, the interfacial strength of the hybrid composite with patterned sheet was not reduced. On the other hand, the failure mode was different. In the case with plain insert, complete pull-out/delamination was achieved and the insert was not damaged at any location. The maximum force in the force-displacement curve was influenced only by the delamination behavior and damage initiation. In the case of patterned sheet, there was no delamination in the specimen, except a very thin region near the lower edge, and the specimen failed due to the breakage of the thin strands of the pattern on the insert, as it is shown in Fig. 4.

If there are through micro-cuts in the insert, apart from shear stress along the interface between the insert and bulk matrix, the hard contact developed among the insert and matrix material on the inner surface of the holes, is also responsible for the load transfer in tensile loading. As a result, the overall load transfer capacity and interfacial strength of the hybrid composite is improved.

3.2. Dynamic tests

A series of impulse tests were conducted to evaluate the improved structural damping of the SMA-GFRP hybrid composite with sheet inserts of *CuZnAl* with micro-cuts having the architecture of Fig. 1, and the shape of a slender beam. The hybrid composite specimen had 205 mm length, rectangular cross-section with 27 mm width and 5 mm thickness, and a thick core of GFRP $[+45/-45]_{11}$. For comparison, dynamic tests were also performed on a twin specimen made of GFRP $[+45/-45]_{15}$ without SMA inserts. Each of the two beam specimens was set-up in a cantilever configuration (Fig. 5), mounted to have 175 mm free length. An impulse load was applied by means of a modally tuned Impulse Hammer, and damping ratio was evaluated from the free response. Each test was repeated nine times and the displacement of the free end (Point 1 in Fig. 5) was measured with a triangulation laser (MEL-M7L/20, with measuring range 20 mm and resolution 0.9 μm). Another laser displacement sensor was used to ensure complete fixture of the clamped end (Point 2 in Fig. 5) when the impulse was applied at the free end.

The signals from the hammer and the two laser sensors were acquired by a data acquisition set-up. The real time displacement vs time data at the free end of the specimen is shown in Fig. 6. Further elaboration of the data was done by a MatLab code to evaluate damping ratio. Using Fast Fourier Transform, the spectrum of the

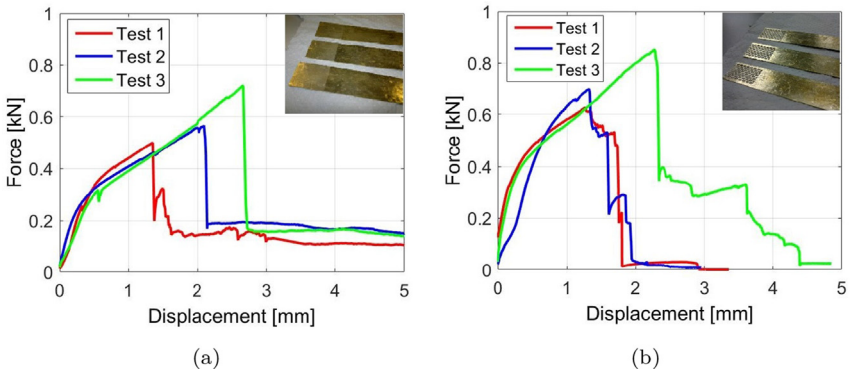

Fig. 3. Pull-out test results of specimens: (a) with plain/uncut insert; (b) with micro-cuts pattern insert.

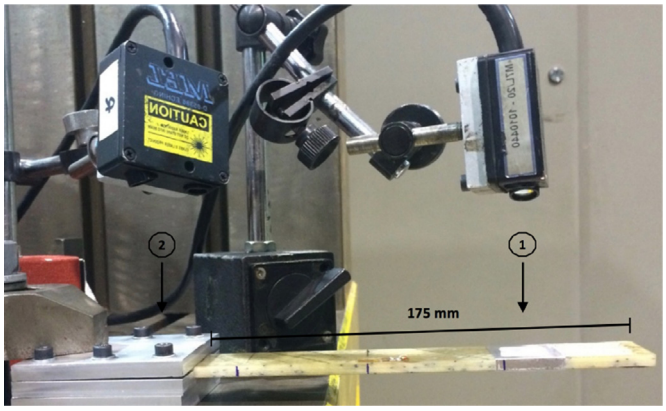

Fig. 5. Experimental set-up for dynamic tests.

signal was filtered and the signal portion of interest was obtained. It was noted that the displacement amplitude decreased in an exponential manner and the rate of amplitude reduction was proportional to the damping property of the specimen. The damping at the dominant frequency can be determined from the envelope (converted into logarithmic scale) of the associated impulse response function. The various steps of this process are shown in Fig. 6. The first natural frequency and damping ratio (**h**) of each sample is reported in the Table 2. The values of the first natural frequency and damping ratio for each sample are reported as the averages with the standard deviation.

The damping ratio of the hybrid composite was found to be 72% more as compared with GFRP specimen and the hybridization by SMA inserts with micro-cuts, according to one of the requirements, does not affect significantly the first natural frequency of the beam specimen. This is important because the hybrid composite was originally proposed for lateral horns of a pantograph's collector, which acts as an auxiliary mass.

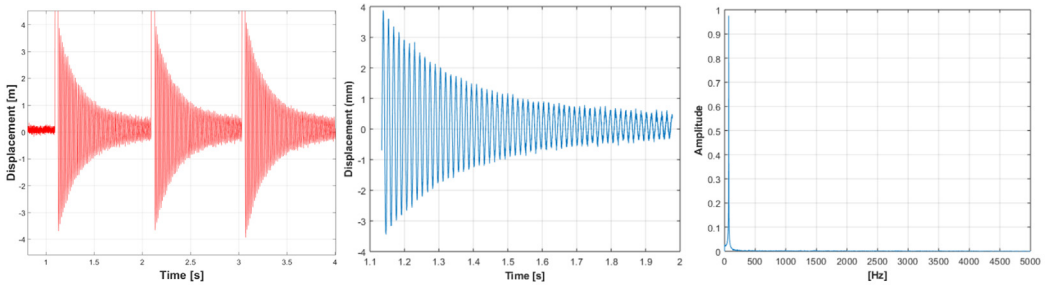

(a) Original signal. (b) Selected displacment time history. (c) Spectrum of the selected displacement time history.

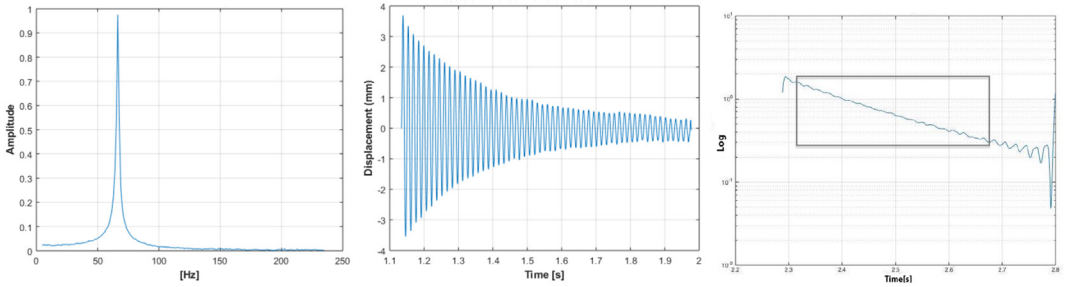

(d) Selected frequency band from the spectrum(c). (e) Result of inverse fft. (f) Module of the hilbert transform in log scale.

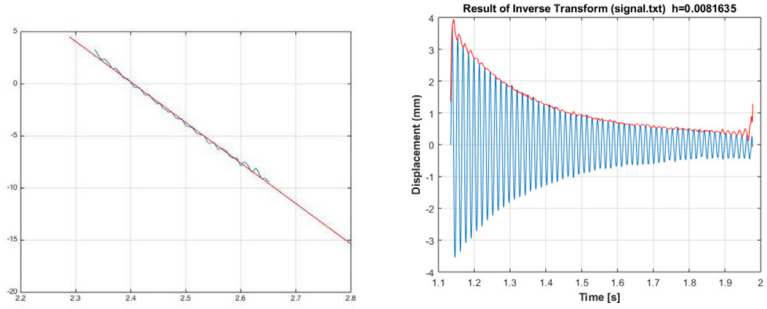

(g) Selected portion of (f) with fitting line. (h) Final result with module of hilbert transfor as envelope of the signal.

Fig. 6. Various steps of calculating non-dimensional damping from the acquired data signal.

Table 2
Experimental values of first natural frequency and damping ratio for the SMA-GFRP hybrid composite and for the GFRP cantilever beam specimens.

Specimen	$f_{n1}[Hz]$		h [%]	
	Mean	Std. dev	Mean	Std. dev
SMA-GFRP	69.23	0.74	0.859	0.012
GFRP	68.50	0.36	0.504	0.016

4. Numerical simulations

4.1. Formulation of the cohesive damage model

Cohesive Damage Models are extensively used to study delamination. Here, *Cohesive Zone Model* (CZM) related to *Cohesive Damage Models* is used to formulate the interface between SMA and GFRP in the hybrid composite.

Cohesive crack model of the interface provides the basis for the *Cohesive Zone Model* (CZM) for the numerical simulation of delamination, with the development of a cohesive damage zone at the crack front, where there are displacement and stress singularities due to both the material and the geometrical discontinuities [12,13]. Cohesive damage models allow a mesh-independent account of material softening, even though they cannot be referred to as non-local damage models [14], assuming that the mesh is refined adequately. CZM formulations allow the provision of both crack initiation and crack propagation, and thus, damage tolerance and interface strength analyses can be done with the same designing tool.

CZM is established on the assumption that the stress transferability between the two parting surfaces does not deteriorate totally at damage initiation, but instead is a continuously growing action controlled by progressive interfacial stiffness reduction [15]. This method is able to represent the delamination physics and can be used to formulate zero thickness cohesive element for FEA simulations. The cohesive behavior is described by elements with initially coincident opposite nodes, that can separate when experience shear or tensile stresses.

As the starting thickness of the cohesive element is 0, the deformation state can not be presented by the usual definition of strain. Instead, separation (mode I) or sliding (mode II & III) δ between the faces connected through the cohesive surface, is used for measuring deformation and (σ - δ) traction-separation relation is used in place of the classical (σ - ε) equation [16]. During the deformation, the resulting separation between adjacent nodes connected through cohesive elements is proportional to the stiffness of the cohesive elements. When the area under the traction-separation curve is equal to the fracture toughness G_c of the interface, the stress is reduced to 0 and fresh crack surfaces originate. In this approach, fracture energy and the critical energy release rate used in linear elastic fracture mechanics is the same.

The cohesive interface element with no thickness is available in *Abaqus* code through a surface interaction with cohesive behavior [17,18]. The interface element can be visualized as a spring between the initially coincident nodes of the element. However, the stiffness of the interface element is part of the structural stiffness, and the interface element will undergo deformation during the loading of the laminate. The initially coincident nodes will open (mode I: opening) or slide (mode II: shear and III: tearing) relative to each other. The nodal separations of the interface elements are always known by solving the discretized structure [5,19].

In the following sections, the discussed FE models uses a bilinear cohesive law (Fig. 7) [20,21]. The relative displacement between the corresponding points across the opposing surfaces of the interface

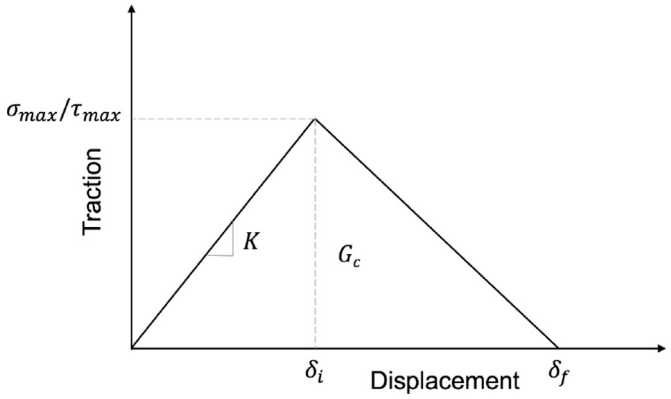

Fig. 7. Bilinear traction separation response for cohesive zone model.

is denoted as δ. The elastic traction-separation behavior can be represented as

$$\begin{bmatrix} \sigma_n \\ \tau_s \\ \tau_t \end{bmatrix} = \begin{bmatrix} K_{nn} & K_{ns} & K_{nt} \\ K_{ns} & K_{ss} & K_{st} \\ K_{nt} & K_{st} & K_{tt} \end{bmatrix} \begin{bmatrix} \delta_n \\ \delta_s \\ \delta_t \end{bmatrix} \quad (1)$$

where: K denotes interfacial stiffness, n denotes normal direction, s denotes shear direction 1 (mode II) and t denotes shear direction 2 (mode III).

Since the proposed hybrid composite is to be used in transverse vibration condition, mode II delamination failure of the interface is representative of the actual service conditions (bending). According to this loading condition, an uncoupled behavior can be assumed. A pure shear slip does not induce cohesive forces in the normal direction, nor does pure normal separation induce cohesive forces in the shear direction 1 or 2. The cohesive behavior can be specified simply by generating penalty contact terms that imposes the cohesive constraint in tangential and normal directions. In eq. (1), K_{nn}, K_{ss} and K_{tt} are used and calculated, while mixed mode stiffnesses are assumed zero.

The tangential interfacial stiffness (K_{ss} and K_{tt}) is derived from the pull-out tests with plain SMA sheet (Fig. 3a), by considering the value of the maximum contact shear stress at the interface (τ_{max}) and the corresponding displacement jump (δ_i). The maximum shear stress can be evaluated by considering the peak force (F_{max}) along with the contact area (A_{cont}) between the GFRP and SMA components:

$$K = \frac{\tau_{max}}{\delta_i} \quad \text{where} \quad \tau_{max} = \frac{F_{max}}{A_{cont}} \quad (2)$$

Table 3 shows the values of τ_{max} at the interface and K_{ss}, derived as the average of the three pull-out tests with plain sheet inserts of Fig. 3a.

The failure of the interface adhesion and thus delamination can be modeled by defining a *Damage initiation criterion* and a *Damage evolution law*. According to the bilinear traction-separation cohesive law, upon loading the response of the interface is linear up to a maximum value of stress or contact separation at the interface

Table 3
Average maximum interface shear stress, and interfacial stiffness for mode II, for pull-out tests with plain sheet inserts.

$\tau_{max}[N/m^2]$	5.0×10^5
$K_{ss}[N/m^3]$	2.50×10^8

when the *Damage initiation criterion* is fulfilled (Fig. 7). In this work, the maximum stress criterion is used:

$$max\left\{\frac{\langle\sigma_n\rangle}{\sigma_n^o}, \frac{\tau_s}{\tau_s^o}, \frac{\tau_t}{\tau_t^o}\right\} = 1 \tag{3}$$

When the damage start/initiation criterion is met, the degradation of the interfacial adhesion initiates, and the degradation rate of the interface stiffness is defined by the *Damage evolution law*. Using assumption of un-coupled modes, the failure of adhesion for any contacting pair of the cohesive interaction can be characterized by a scalar damage variable D, with zero as starting value. When the damage initiation criterion is fulfilled, D starts changing from zero to unity depending on damage evolution law. Damage evolution can be defined by interfacial fracture toughness (G_c). Following the bilinear traction-separation behavior shown in Fig. 7, the interfacial fracture toughness can be calculated as $G_{IIc} = 1/2\tau_{max}\delta_f$, and the following relation is used to represent the evolution of the damage variable D:

$$D = \frac{\delta_f(\delta_{max} - \delta_i)}{\delta_{max}\left(\delta_f - \delta_i\right)} \quad \text{with} \quad \delta_f = \frac{2G_c}{\tau_{max}} \tag{4}$$

where δ_{max} is the maximum value of the effective separation during the load history. Using the derived value for each test (Fig. 3a), $G_c = 900\ J/m^2$ was adopted.

4.2. Modeling of hybrid composite interface having SMA plain sheet insert and mode II delamination

The pull-out test for the composite specimen having plain SMA sheet insert was simulated by setting up a finite element (FE) model (Fig. 8a). The GFRP bulk was defined by isotropic material with elastic properties reported in Table 1. The behavior of the *CuZnAl* alloy was described as elasto-plastic material with the elastic properties of Table 1 and with plastic deformation data from the experimental true stress-strain curve (Fig. 9).

Linear shell elements with reduced integration (S4R) were used to mesh SMA sheet, while linear solid elements with reduced integration (C3D8R) were used for GFRP. A uniform mesh size of 1 mm was selected after checking for mesh convergence. GFRP parts and SMA sheet were connected through a surface-to-surface

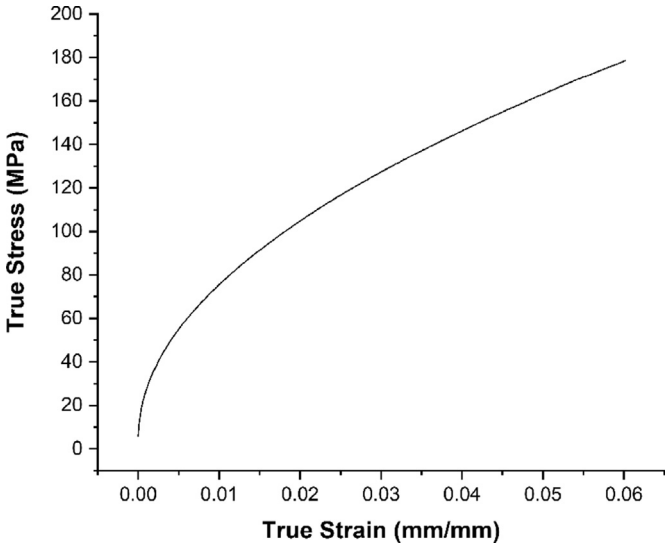

Fig. 9. True Stress-strain graph for *CuZnAl* SMA.

interaction with cohesive and damage properties, according to the cohesive model discussed in the previous section. It is suggested in Ref. [17] to use zero for *penalty* stiffness in the normal direction when there are no applied forces in this direction. Of course, some force are generated in the normal direction as well due to Poisson's effect and using zero value results in convergence problems. Therefore, a value of $1 \times 10^{12}\ N/m^3$ was chosen for *penalty* stiffness in normal direction.

Displacement load along Y direction was applied to the lower faces of the GFRP components and the bottom end of the SMA sheet was fixed, as shown in Fig. 8a. The force-displacement graph was plotted by recording the reaction force at the fixed end of the SMA sheet.

Stiffness calibration was performed by comparing the rising part of the force displacement curve of the simulation with experimental results. The calibration plot for a test is reported in Fig. 8b. The average of the optimal values of tangential interfacial stiffness for the SMA-GFRP cohesive model are reported in Table 4. It must be noted here that the cohesive model applied here is mesh

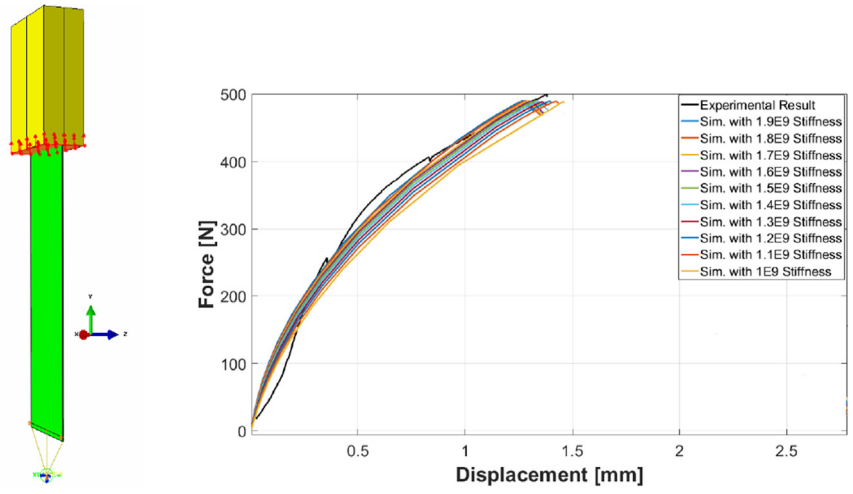

Fig. 8. (a) Model for pull-out test simulation with plain SMA sheet insert. (b) Numerical calibration of the tangential interfacial stiffness for Test 1 with plain sheet.

Table 4
Numerical results for tangential interfacial stiffness, maximum force, numerical displacement jump at the maximum force, and minimum force for the damage initiation, for pull-out test with plain sheet insert.

$K_{ss,num}$ [N/m^3]	1.07×10^9
$F_{max,num}$ [N]	581
$\delta_{i,num}$ [mm]	2.07
F_d [N]	494

independent and the relations used to calculate interfacial parameters contain no penalty or mesh dependent term (eqs. (2) and (4)). This is only true for mode-II delamination, which is under study here.

Slip condition at the interface and final complete delamination was observed in the simulation, as in the experiment tests.

The simulation results allowed to calculate the minimum force (F_d) corresponding to the start of interfacial degradation. To determine it, the damage initiation criteria was plotted versus displacement, for every contact node pair. The value of F_d was obtained by tracing the force on the force displacement graph when the damage criterion was fulfilled for the first contacting node pair, as shown in Fig. 10. It can be observed that the results are strongly affected by the non-linearity of the SMA material and for this reason, F_d is higher than the load at the deviation from linearity, and close to the maximum load and therefore, can not be taken from the experimental results as the load at the deviation from linearity.

4.3. Modeling of hybrid composite interface having SMA sheet insert with micro-cuts

The pull-out test for the hybrid composite having SMA insert having micro-cuts was simulated by setting up a finite element (FE) model (Fig. 3b). The general dimensions of the model, constraints on SMA sheet end and displacement load on GFRP faces, were defined exactly the same in the case of specimen with plain SMA insert.

The presence of micro-cut pattern requires, instead, a more detailed modeling of the interface between GFRP and SMA insert, as shown in the exploded view of the model (Fig. 11). To reduce simulation duration, the GFRP blocks were split into two parts, one having coarse mesh and other having fine mesh that comes in contact with the SMA sheet which were then tied together. GFRP-

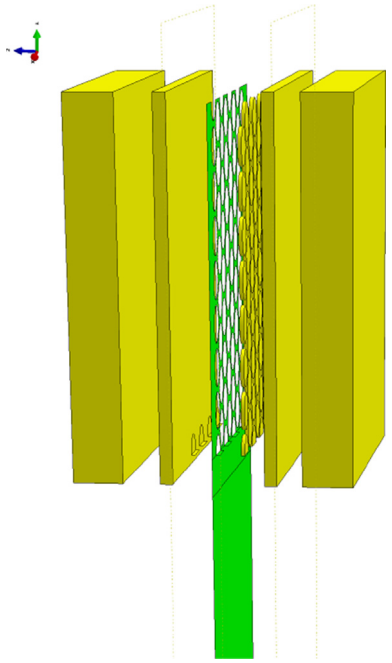

Fig. 11. Exploded view of the model with *CuZnAl* SMA insert having micro-cuts.

SMA interaction is considered along the parallel faces like in the case of plain insert, as well as along the inner surface of the micro-cuts.

As per the general recommendations for interacting surfaces, finer mesh was used on the *Slave* surface and in the case that contacting surfaces have same mesh density, the surface with softer underlying material was chosen as *Slave* [17]. Same interface parameters were used for defining cohesive interaction between GFRP parts and SMA sheet insert, as in the case of plain insert. Interface parameters like *Cohesive behavior* and *Damage* were the averages of tangential interfacial stiffness equal to $1.07 \times 10^9\ N/m^3$ and of maximum shear stress equal to $4.96 \times 10^5\ N/m^2$, with $G_c = 900\ J/m^2$. In all these interactions, discretization method was chosen to be *Node-to-surface* and sliding formulation as *Small sliding* due to the interaction between edges and surfaces and the inherent non-linear behavior of the analysis.

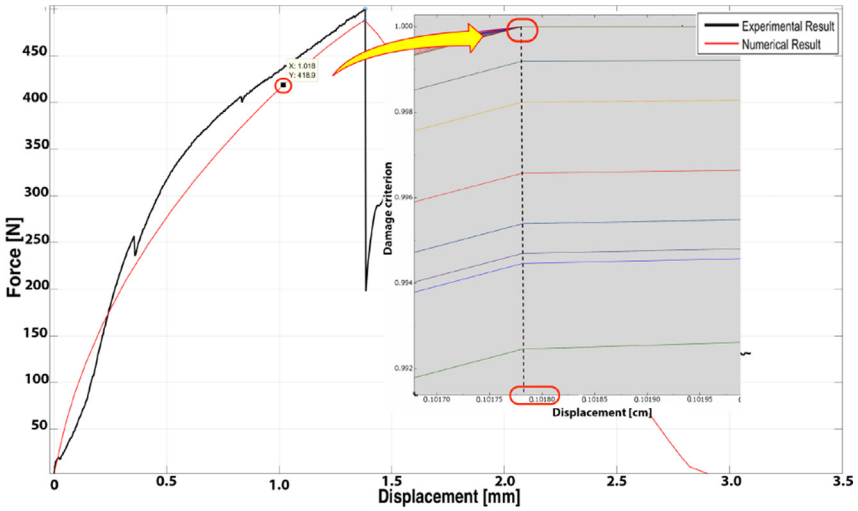

Fig. 10. Calculation method for minimum force required for damage initiation F_d, for specimen with plain sheet insert.

The important point to be discussed here is that, as in the pull-out experiments with specimen having micro-cut insert, the FE analysis predicted the failure of the SMA sheet at the thin strands between the first line of elliptical holes and no delamination and failure of cohesive interaction between the patterned SMA insert and the GFRP was observed (with the exception of a thin region near the bottom edge of the SMA-GFRP sandwich). It is to be noted that the profile of the failed specimen in the simulation results is exactly the same as the experimental one (Fig. 12).

Fig. 13 shows that the damage initiation criterion, for all nodes on the SMA-GFRP interface, is farther from being met and interface damage does not occur. In addition, the gradient of the curves in the *Damage initiation criterion* plot is diminished to right around zero after some displacement, suggesting it is unlikely that the interface will be damaged on additional loading. This outcome is fully in-accordance with the experimental findings and the requirements for better adhesion between the GFRP host and the SMA insert.

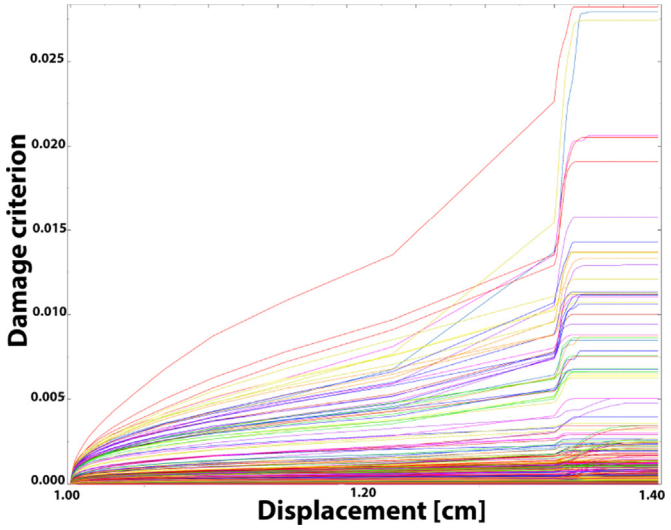

Fig. 13. Plot of damage initiation criterion versus applied displacement all the contact nodes at the *CuZnAl* SMA-GFRP interface.

4.4. Numerical simulation of the hybrid composite dynamic behavior

The FE model for numerical simulation of the hybrid composite's dynamic behavior is comprised of a core GFRP bulk with a layer of SMA insert on top and bottom. The dimensions of the model are exactly the same as the specimen used for experimentation.

The materials were modeled as in the FE analysis of the pull-out test. The bulk GFRP core ($205 \times 27 \times 4.6$ mm^3) was modeled as elastic homogeneous solid with properties reported in Table 1, while the SMA inserts ($200 \times 23.5 \times 0.2$ mm^3) were modeled as elasto-plastic shells with elastic properties reported in Table 1, and with true stress-strain behavior obtained from tensile test.

The interaction between the GFRP core and the SMA layers was modeled by using two different approaches:

1. *Tie* constraint between *CuZnAl* SMA sheet and GFRP core;
2. Cohesive surface model for the interface of *CuZnAl* SMA-GFRP validated from the numerical simulation of pull-out tests.

One end of the SMA-GFRP beam was clamped by using *Encastre* on top and bottom surfaces, up to 30 mm out of 205 mm in length, to have a free length of 175 mm of the specimen in cantilever configuration.

The FE model was first used for Eigenfrequencies extraction analysis and evaluation of the damping ratio using Modal Strain Energy (MSE) procedure, and then for Modal Dynamics analysis and related damping ratio evaluation.

4.5. Eigenmodes extraction and Modal Strain Energy procedure

The first natural frequency of the hybrid composite beam in the cantilever configuration comes out to be 79.9 Hz if *Tie* constraint is used to model the interaction between GFRP core and the SMA layers, while it is 69.4 Hz if the cohesive surface model is used instead (Table 5). The flexural stiffness of the beam hybrid composite is clearly overestimated when the *Tie* constraint is introduced, while the cohesive surface model allows an adequate modeling of the effective flexural stiffness of the composite.

The linear elastic, undamped, modal finite element analysis for the natural frequencies extraction allows, also, the calculation of the strain energy ratio of each component for the first modal shape in order to evaluate the damping ratio of a layered composite according to the Modal Strain Energy procedure:

$$\mathbf{h} = \Sigma_{i=1}^{N} \alpha_i h_i \tag{5}$$

where:

$\mathbf{h}$ = Damping ratio for the composite.

α_i = The ratio of elastic strain energy/total elastic energy for each component of the composite.

h_i = Damping ratio for each component of the composite.

N = Number of components.

Table 5
First natural frequency of the hybrid composite, strain energy ratio and damping ratio for each component of the hybrid composite, and total damping of the hybrid composite calculated by MSE procedure.

	Composite	GFRP		SMA		Composite
	$f_{n,1}$ [Hz]	α[%]	h [%]	α[%]	h [%]	h [%]
Tie constraint	79.9	81.15	0.50	18.85	3.7	1.11
Cohesive model	69.4	98.66		1.34		0.54

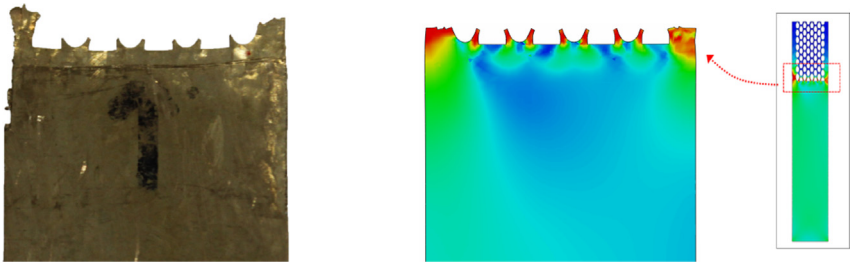

Fig. 12. Comparison between numerical and experimental profile of the failure for the pull-out test elliptical holes patterned sheet.

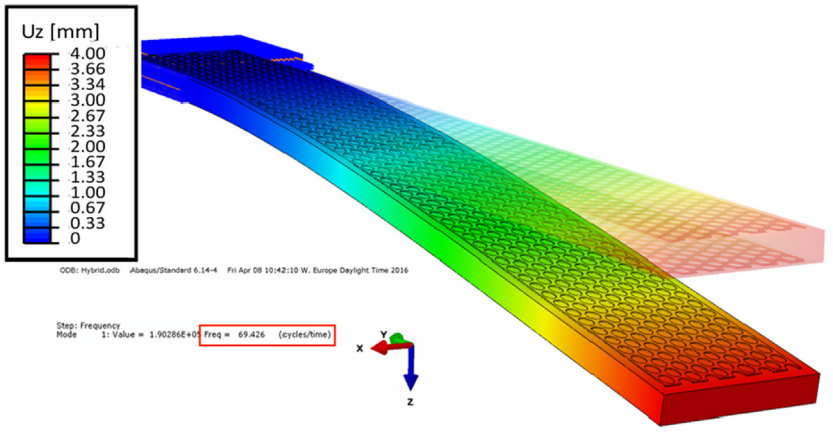

Fig. 14. Displacement field associated at the first modal shape of the SMA-GFRP hybrid composite.

The strain energy ratio of GFRP and SMA are reported in Table 5, for the two different approaches used to model the interaction between the GFRP core and the SMA layers. Using cohesive surface model for the interaction between GFRP core and the SMA layers, the stiffness of the interface is reduced and the ratio of elastic strain energy versus the total elastic energy stored in the SMA insert significantly decreases.

An appropriate value of the damping ratio for GFRP component, strongly dependent on the frequency, is assumed from the value obtained by dynamic test on the GFRP beam (Table 2 and reported in Table 5), while in order to consider an appropriate value for *CuZnAl* SMA alloy, strongly dependent on the strain amplitude, an average strain amplitude in the SMA material was calculated. The average strain amplitude is the value corresponding to the first modal shape of Fig. 14, where the displacement of the free end of beam was 4 mm, comparable with the displacement in the experimental tests. The damping ratio exhibit by the *CuZnAl* SMA alloy, at the average value of the strain amplitude [8], has been used as appropriate value for the MSE procedure and is reported in Table 5.

On this basis, the damping of the hybrid composite was calculated by MSE procedure and reported in the same table, when *Tie* constraint or cohesive surface model is used to model the SMA-GFRP interface. If the case with Tie constraint at the interface is considered, due to the high percentage of strain energy stored in the SMA insert, the total damping of the hybrid composite is significantly increased and even overestimates the experimental value (Table 2). When the cohesive surface model is considered, the strain energy stored in the SMA insert is very low and the increase of the hybrid composite damping predicted by the MSE, with respect to the GFRP matrix, is limited.

4.6. Modal dynamics procedure

The damping property of the hybrid composite with micro-cut patterned SMA sheet inserts was also evaluated by Modal Dynamics analysis. Here, the structure's response is based on the previous eigenmodes extraction, and on displacement-time history response as a linear perturbation procedure using modal superposition. For the application of this procedure, only the case with cohesive surface model for the patterned SMA-GFRP interface was considered.

For defining damping of the *CuAlZn* SMA and GFRP, the strain dependence and frequency dependence was considered respectively, according to Ref. [8]. A impulse load was applied at the free end of the specimen and the free decaying oscillation of the model

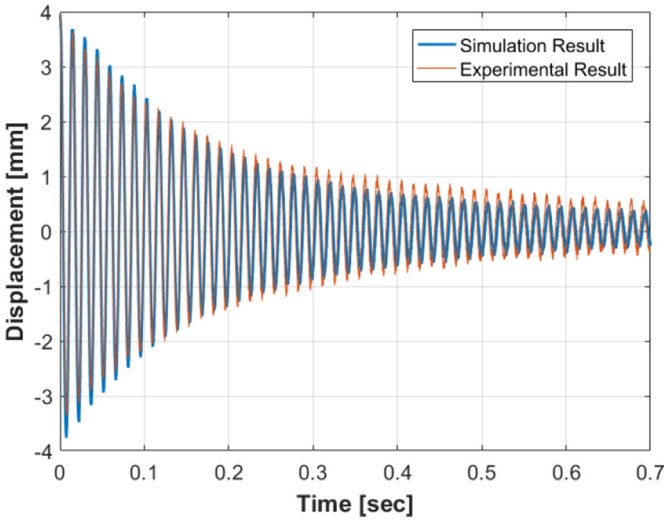

Fig. 15. Numerical displacement history at the free end of the specimen and comparison with the experimental results.

was observed. The peak of the force history was set in order to have the same displacement at the free edge of the specimen as the experimental decay history selected for comparison. The numerical displacement history at the free end of the cantilever configuration is shown in Fig. 15 and compared with the experimental results.

The numerical displacement-time history was analyzed by the same MatLab code used to analyze experimental data, that calculated the damping at the dominant frequency as the envelope of the impulse response function in logarithmic scale. The damping ratio of the hybrid composite beam was found to be 0.85 [%], well in agreement with the average experimental value of Table 2.

It can be observed that the Modal Dynamic procedure, with the cohesive model of the interface between GFRP and SMA insert, allowed to reproduce numerically the experimental dynamic behavior of the *CuZnAl* SMA-GFRP hybrid composite, both in terms of natural frequency and the damping ratio.

5. Conclusions

The interfacial parameters have been derived for simulating delamination during mode-II loading conditions using cohesive

surfaces/interactions, for SMA-GFRP based hybrid composite. Two geometries of the SMA insert are investigated, plain *CuZnAl* SMA sheet insert and *CuZnAl* SMA sheet insert having elliptical micro-cut pattern.

Further it was noted, experimentally and in numerical simulations, that de-bonding does not occur during the pull-out tests for hybrid composite samples with SMA inserts having elliptical micro-cut pattern. Rather, SMA material failed after yielding. In addition, it was demonstrated that using the numerical model the minimum force required for damage initiation at the SMA-GFRP interface can be calculated.

The damping property of the hybrid composite with patterned SMA sheet inserts in the shape of cantilever beam has been experimentally evaluated by impulse excitation tests, and numerically calculated by Modal Strain Energy and Modal Dynamics procedures. Experimental tests have shown that the structural damping of the hybrid composite is 72% more as compared with GFRP specimen and the hybridization by laser patterned SMA insert does not affect significantly the first natural frequency of the beam specimen, as one of the goals of the hybridization was to preserve the weight and natural frequency of the specimen.

The results in terms of first natural frequency and damping ratio by using Modal Strain Energy (MSE) and Modal Dynamics numerical procedures have shown that the Modal Dynamics procedure allowed to produce results that are more in agreement with the experimental results, as compared to MSE approach.

Based on these observations, the effectiveness of the micro-cut patterned SMA sheet insert has been validated to enhance the interface adhesion and damping in the hybrid composite for the proposed application.

Conflicts of interest

The authors declare that there is no conflicts of interest.

Acknowledgements

The authors wish to thank the Composite Materials Laboratory at the Department of Aerospace Engineering of the Politecnico di Milano for the manufacturing of the hybrid composite samples.

References

[1] J. Van Humbeek, S. Kustov, Active and passive damping of noise and vibrations through shape memory alloys: applications and mechanisms, Smart Mater. Struct. 14 (2005) 171–185.
[2] Y. Zhang, Y.P. Zhao, A study of composite beam with shape memory alloy arbitrarily embedded under thermal and mechanical loadings, Mater. Des. 28 (2007) 1096–1115.
[3] Q.Q. Ni, R. Xin Zhang, T. Natsuki, M. Iwamoto, Stiffness and vibration characteristics of SMA/ER3 composites with shape memory alloy short fibers, Compos. Struct. 79 (2007) 501–507.
[4] J. Van Humbeeck, Damping capacity of thermoelastic martensite in shape memory alloys, J. Alloy. Comp. 58 (2003) 58–64.
[5] W. Huang, On the selection of shape memory alloys for actuators, Mater. Des. 23 (2002) 11–19.
[6] M.O. Moroni, R. Saldiviaand, M. Sarrazin, A. Sepúlved, Damping characteristics of a CuZnAlNi shape memory alloy, Mater. Sci. Eng. 335 (2002) 303.
[7] M. Bocciolone, M. Carnevale, A. Collina, N. Lecis, A. Lo Conte, B. Previtali, C.A. Biffi, P. Bassani, A. Tuissi, N. Lecis, Design for damping of a railway collector based on the application of shape memory alloy, Smart Mat. Res. (2012), 797319.
[8] C.A. Biffi, P. Bassani, A. Tuissi, M. Carnevale, N. Lecis, A. Lo Conte, B. Previtali, Flexural vibration suppression of Glass fiber/CuZnAl, Funct. Mat. Lett. 5 (1) (2012).
[9] M. Bocciolone, M. Carnevale, A. Collina, N. Lecis, A. Lo Conte, B. Previtali, C.A. Biffi, P. Bassani, A. Tuissi, Strength of SMA-GFRP interface in a new designed railway collector, in: E. Carrera, F. Miglioretti, M. Petrolo (Eds.), Proceedings of 6th Conference on Smart Structures and Materials, Torino, June 2013, pp. 24–26. www.smart2013.com.
[12] L. Zhao, Y. Gong, J. u Zhang, Y. Chen, B. Fei, Simulation of delamination growth in multidirectional laminates under mode I/II loadings using cohesive elements, Compos. Struct. 116 (2014) 509522.
[13] J.W. Hutchinson, Z. Suo, Mixed mode cracking in layered materials, Adv. Appl. Mech. 29 (1992) 63–191.
[14] M. Jiràsek, Z.P. Bazant, Nonlocal integral formulations of plasticity and damage: survey of progress, J. Eng. Mech. 128 (2002) 1119–1149.
[15] G.A.O. Davies, L. Guiamatsia, The problem of the cohesive zone in numerically simulating delamination/debonding failure modes, Appl. Compos. Mater. 19 (2012) 831–838.
[16] M. Saeedifar, M. Fotouhi, M.A. Najafabadi, H.H. Toudeshky, Prediction of delamination growth in laminated composites using acoustic emission and cohesive Zone Modeling techniques, Compos. Struct. 124 (2015) 120–127.
[17] ABAQUS/CAE user's manual, version 6.14. (2014) by Dassault Systèmes.
[18] M. Ana, Girão Coelho, Finite element guidelines for simulation of delamination dominated failures in composite materials validated by case studies, Arch. Comput. Methods Eng. 2 (2015) 363–388.
[19] S. Jaques, I. De Baere, W. van Paepegem, Analysis of the numerical and geometrical parameters influencing the simulation of mode I and mode II delamination growth in unidirectional and textile composites, Appl. Compos. Mater. 22 (2015) 637–668.
[20] A. Touron, G.D. Davila, P.P. Camanho, J. Costa, An engineering solution for mesh size effects in the simulation of delamination using cohesive zone models, Eng. Fract. Mech. 74 (2007) 1665–1682.
[21] P.W. Harper, S.R. Hallet, Cohesive zone length in numerical simulation of composite delamination, in: Engineering Fracture Mechanics, vol. 75, 2008, pp. 4774–4792.